Characterization of the Metal−Organic Framework Compound Cu_3(benzene 1,3,5-tricarboxylate)$_2$ by Means of ^{129}Xe Nuclear Magnetic and Electron Paramagnetic Resonance Spectroscopy

Winfried Böhlmann,*,† Andreas Pöppl,† Michal Sabo,‡ and Stefan Kaskel‡

Universität Leipzig, Fakultät für Physik und Geowissenschaften, Linnéstr. 5, D-04103 Leipzig, Germany, and Technische Universität Dresden, Institut für Anorganische Chemie, Mommsenstr. 6, D-01062 Dresden, Germany

Received: May 19, 2006; In Final Form: July 18, 2006

^{129}Xe NMR measurements of adsorbed xenon are shown for the first time to be a suitable tool to characterize the porosity and the properties of the metal−organic framework $Cu_3(BTC)_2(H_2O)_3$ (BTC = benzene 1,3,5-tricarboxylate). The NMR experiments are performed at room temperature and over a wide range of xenon pressure and on two different synthesized $Cu_3(BTC)_2$ samples. ^{129}Xe NMR results reveal that in dependence on the kind of the synthesis pathway either one or two signals are observed which can be attributed to two kinds of fast exchange of xenon atoms in two pores with different pore sizes. Coadsorption experiments of xenon and ethylene demonstrate that the xenon atoms prefer to fill the greater pores of the material because the smaller pores are occupied with residual molecules from the synthesis procedure and additionally adsorbed ethylene. Besides the NMR experiments a series of electron paramagnetic resonance (EPR) measurements are performed to estimate the state of copper having a strong influence on the chemical shift of the adsorbed xenon. The EPR experiments demonstrate that spin exchange between the interconnected copper dimers is taking place across the BTC linker molecules in the $Cu_3(BTC)_2$ framework.

Introduction

In 1997 Yaghi et al.[1,2] described a synthesis of coordination polymers based on metal zinc employing bi- to tetravalent aromatic carboxylic acids which they designated as metal−organic frameworks (MOFs). Nowadays several hundred different MOFs are known where as well as the metal and/or the organic linker are modified. These compounds have received a great deal of attention due to their potential application as gas storage media and catalyst material,[3−5] respectively. The materials composed of an organic linker and a metal complex or cluster possess properties such as a drastically increased velocity of molecular traffic[6] through the open structures, a high micropore volume, and high surface areas. Therefore, this combination of a wide chemical inorganic−organic composition makes these substances interesting for many research groups in both academia and industries.[7,8]

Most of these studies describe new synthesis strategies, the characterization of the materials by X-ray diffraction (XRD), IR and UV/VIS spectroscopy, nitrogen adsorption−desorption measurements, and first attempts to store different gases such as hydrogen[9,10] and carbon dioxide.[11] To our knowledge only a few studies exist[5,12,13] dealing with NMR experiments to obtain more information about the structure and the behavior of guest molecules inside the pores.

It is well known that xenon is an ideal probe to investigate the properties of porous materials such as zeolites,[14−16] porous carbons,[17,18] and microporous polymers.[19,20] A high polarizability of the xenon electron cloud makes it very sensitive to physical interactions with its environment resulting in a wide ^{129}Xe NMR chemical shift range. Therefore, we used the ^{129}Xe NMR spectroscopy to investigate the pores of the MOF $Cu_3(BTC)_2$.[21] The obtained ^{129}Xe NMR shifts are the weighted average of several types of interactions on the NMR time scale. From the pioneer work of Fraissard and Ito,[14,15] it is known that the chemical shift δ of adsorbed xenon is the sum of different terms corresponding to various interactions

$$\delta = \delta_0 + \delta_S + \delta_{Xe-Xe\rho Xe} + \delta_E + \delta_M + \delta_{SAS} \qquad (1)$$

where δ_0 is the reference shift, $\delta_{Xe-Xe\rho Xe}$ arises from the Xe−Xe collisions and is expected to vary linearly with the xenon density at low xenon loading and it shifts to higher values with increasing the xenon concentration. The term δ_E is the shift due to the electric field caused by cations in the porous material, δ_M describes an extra term accounting for the presence of paramagnetic centers, δ_{SAS} belongs to the shift of strong adsorptions sites, and δ_S reflects the interactions of the xenon atoms with the surface. Latter is related to the dimension and the shape of the pores by means of the mean free path l of the adsorbed xenon. The larger these dimensions and/or the easier diffusion inside the pores, the smaller the δ_S value.[22]

Thus, in the present work we first describe a characterization of the porosity and the influence of framework composition of this MOF by means of ^{129}Xe NMR spectroscopy. Consequently, we measured ^{129}Xe NMR spectra of a wide pressure range. Additionally, coadsorption experiments are also studied in order to estimate the size of micropores in $Cu_3(BTC)_2$. Besides the NMR studies some electron paramagnetic resonance (EPR) measurements are performed to characterize the state of copper into the framework.

* To whom correspondence should be addressed. E-mail: bohlmann@physik.uni-leipzig.de. Fax: +49-341-9732649. Phone: +49-341-9732613.
† Universität Leipzig.
‡ Universität Dresden.

10.1021/jp063074r CCC: $33.50
Published on Web 09/09/2006

Experimental Section

Synthesis. $Cu_3(BTC)_2$ was synthesized according to the procedure described elsewhere.[21]

Sample A. In a typical synthesis, 0.875 g (3.6 mmol) of $Cu(NO_3)_2 \cdot 3H_2O$ were dissolved in 12 mL of deionized water and mixed with 0.42 g (2.0 mmol) of trimesic acid dissolved in 12 mL of ethanol. The solution was filled in a 40-mL Teflon liner, placed in an autoclave, and heated to 120 °C for 12 h.

Sample B. $Cu(NO_3)_2 \cdot 3H_2O$ (10.39 g; 43.00 mmol) was dissolved in 83.30 mL of water, and trimesic acid (5.00 g; 23.79 mmol) was dissolved in 83.30 mL of dimethylformamide (DMF). To each solution, 41.70 mL of ethanol was added; then both solutions were mixed together (250 mL of reaction solution) and kept in a 1-L HDPE jar and stirred for 10 min. The tightly capped vessel was heated at 85 °C for 18 h and then cooled for 8 h to room temperature. The blue crystals were washed with DMF and exchanged with dichloromethane three times (3×200 mL CH_2Cl_2) in 3 days. The dark blue crystals were isolated and evacuated at 180 °C for 48 h.

XRD. XRD patterns were recorded in transmission geometry using a STOE Stadi-P diffractometer and Cu Kα_1 radiation ($\lambda = 0.15405$ nm).

Thermal Analysis. The thermogravimetric mass spectrometry measurements were carried out in air using a Netzsch STA 409PC thermobalance.

NMR Measurements. For the ^{129}Xe NMR measurements the $Cu_3(BTC)_2$ material was outgassed under vacuum for 48 h at 200 °C. After the samples were cooled to room temperature, xenon gas with a known pressure was condensed by cooling the material with liquid nitrogen. Finally, the NMR glass tubes were flame sealed. The obtained samples were measured at a resonance frequency of 138.29 MHz on a Bruker MSL 500 spectrometer. The ^{129}Xe NMR spectra were performed using a 90° pulse length of 5.9 μs, a recycle delay of 4 s, and magic angle spinning (MAS) with a rotation frequency of 4 kHz. Typically, 1000 scans were performed to obtain a good signal-to-noise ratio. At least 4000 scans were accumulated at xenon loading pressures lower than 40 kPa. The xenon chemical shifts were referenced to the chemical shift of xenon gas extrapolated to zero pressure.

The samples of coadsorption of Xe and ethylene were prepared in a similar manner. After the dehydration at 200 °C under vacuum conditions a known amount of ethylene was adsorbed and then the same pressure of xenon gas was frozen onto the sample with liquid nitrogen. Before NMR measurements, the samples were kept at room temperature for a few days in order to allow the gases a homogeneous distribution over the material.

EPR Measurements. For EPR measurements the samples were transferred into EPR quartz tubes and evacuated for 48 h at 80 °C and finally sealed. EPR spectra were recorded with an X-band ESP 300 ($n_{mw} = 9.4$ GHz) BRUKER spectrometer. The magnetic flux density B_0 of the magnet coils used for the EPR experiments was calibrated by ^{1}H NMR MJ110R magnetometer. During measurements the temperature was controlled by an Oxford ESR 900 He flow cryostat.

Results and Discussions

By consideration of the terms in eq 1, thus it is seen that the chemical shift of the adsorbed xenon depends on several parameters in the porous system. In the case of the $Cu_3(BTC)_2$ material one can expect a great contribution of the δ_M describing paramagnetic centers which are given here in the presence of Cu^{2+} ions. Furthermore, residual water and solvent molecules such as DMF deriving from the synthesis should have a strong influence due to the chemical shifts.

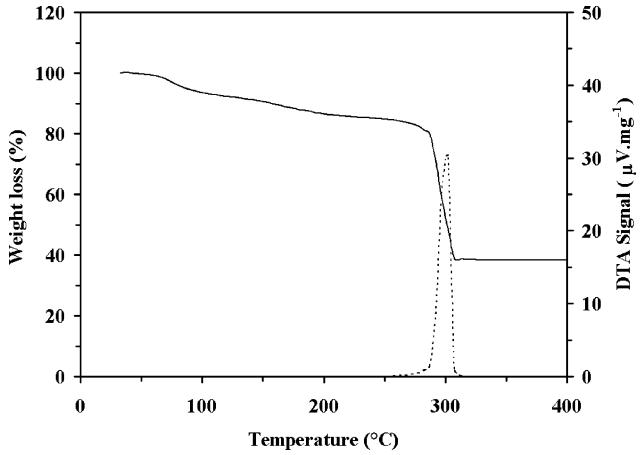

Figure 1. Thermal gravimetric (solid line) and differential thermal analysis (dashed line) of $Cu_3(BTC)_2$ sample A.

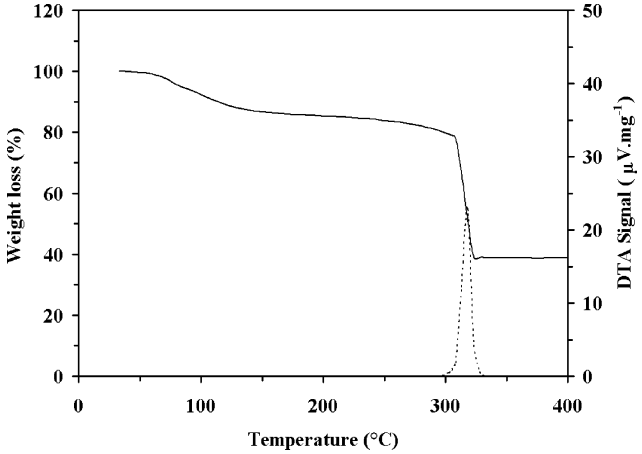

Figure 2. Thermal gravimetric (solid line) and differential thermal analysis (dashed line) of $Cu_3(BTC)_2$ sample B.

Both samples are characterized using thermal gravimetric measurements coupled with a mass spectrometer. In Figure 1, the results are shown for sample A indicating a weight loss of 14.6 wt % up to 200 °C. The latter is mainly due to dehydration according to mass spectrum (*m*/*z* 18). At 302 °C decomposition of the $Cu_3(BTC)_2$ framework causes further weight loss (mass fragments: *m*/*z* 18 for water, 44 for CO_2, and 78 for benzene rings). The thermal analysis of sample B reveals only small differences in thermal analysis and the mass spectrum (Figure 2). In a first step (up to 253 °C), sample B loses 16.2 wt %. This is similar to the mass loss of sample A. However, in this step, mass fragments of CH_2Cl_2 (*m*/*z* 84), DMF (*m*/*z* 42 and 45, respectively), and also water (*m*/*z* 18) can be observed. The framework starts to decompose at about 308 °C (exothermal maximum at 318 °C). In this step, the same mass fragments are observed with *m*/*z* 18 for water, 44 for CO_2, 78 for benzene rings, and the fragments *m*/*z* 42 for N═C═O· and 45 for $(CH_3)_2$-NH for DMF. These results indicate that according to the synthesis procedure small molecules such as CH_2Cl_2, DMF, and water are occupying the pores in sample B, whereas in sample A only water is adsorbed. The latter is the reason for the differences in the pore size distributions observed since DMF has a high boiling point and is probably not completely removed in the activation procedure thus blocking the smaller pore in $Cu_3(BTC)_2$.

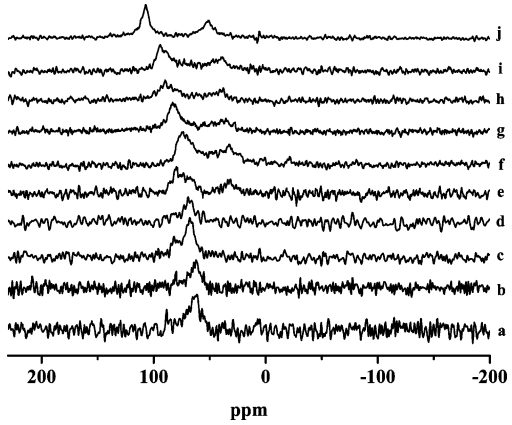

Figure 3. Pressure-dependent ^{129}Xe NMR spectra (performed at room temperature) of xenon adsorbed on $Cu_3(BTC)_2$ sample A: (a) 5, (b) 10, (c) 20, (d) 30, (e) 40, (f) 60, (g) 80, (h) 100, (i) 130, and (j) 150 kPa.

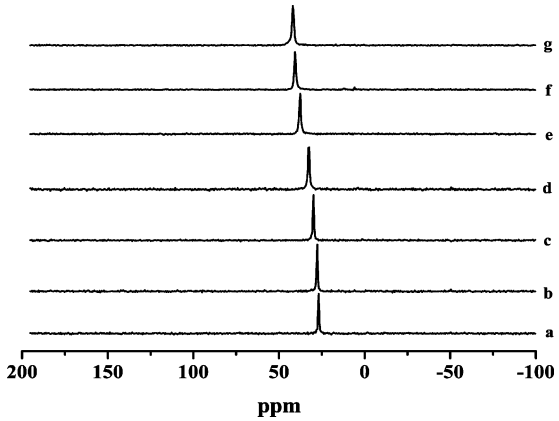

Figure 4. Pressure-dependent ^{129}Xe NMR spectra (performed at room temperature) of xenon adsorbed on $Cu_3(BTC)_2$ sample B: (a) 20, (b) 40, (c) 60, (d) 80, (e) 100, (f) 130, and (g) 150 kPa.

Judging from the powder patterns only minor differences in some peak intensities are observed for samples A and B as compared with the calculated powder pattern (not shown here). However, in the calculation, loading of the pores with different solvent molecules is not taken into account. Therefore, in all samples identical framework structures are present but samples A and B differ in the number and composition of adsorbed molecules.

Actually, one can assume that the results mentioned above and the presence of paramagnetic ions into the framework of the MOF have a strong influence on the line width and the position of the xenon signals. Therefore, we applied MAS NMR experiments for all xenon-loaded samples described in this study. It is well-known that the MAS method contributes to a averaging of chemical shift anisotropy resulting in a better resolution and a line narrowing. Figure 3 shows the ^{129}Xe NMR spectra of xenon adsorbed in $Cu_3(BTC)_2$ sample A with varying adsorption pressures of xenon from 5 to 150 kPa. No ^{129}Xe signal arising from free xenon gas can be detected, which is likely due to the rapid exchange between xenon atoms in the interparticle space and the pores of the MOF. At all loading pressures two signals are detected, which are a hint to two different pore sizes. It is established[15,22] that the larger the pore size, the smaller the value of δ_S. Therefore, the signal at lower chemical shift values can be assigned to the larger pores of the $Cu_3(BTC)_2$ (line a in Figure 4). In the pressure range between 5 and 40 kPa an increase of the chemical shift of this peak is obtained up to xenon pressure

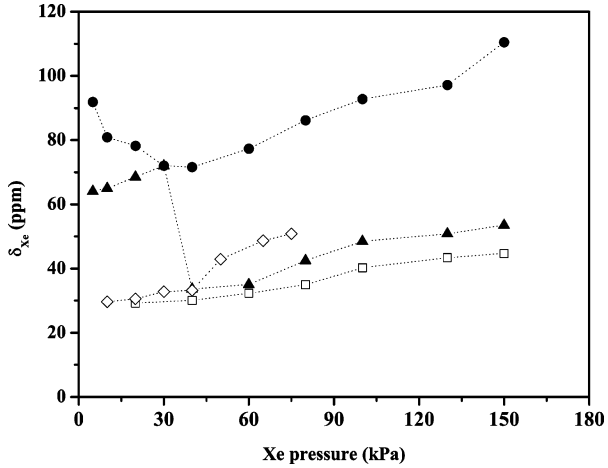

Figure 5. ^{129}Xe NMR shifts plotted against corresponding xenon pressures: (▲ line a) $Cu_3(BTC)_2$ sample A, (● line b) $Cu_3(BTC)_2$ sample A, (□) $Cu_3(BTC)_2$ sample B, and (◇) xenon coadsorbed with ethylene on $Cu_3(BTC)_2$ sample B.

of 40 kPa. A further increase of the xenon pressure leads to a decrease in chemical shift value of about 30 ppm and a loss in intensity. It seems that at lower xenon loadings most of the atoms are preferably adsorbed in the larger pores of the $Cu_3(BTC)_2$ which is also demonstrated in the higher intensity of the peak compared with the signal (line b in Figure 4) assigned to xenon adsorbed into the smaller pores. At higher xenon pressures the MOF shows the typical behavior as it is known from zeolites having two different pore sizes.[23,24] The chemical shift of the peak assigned to the smaller pores follow a parabolic correlation against the adsorption pressure of the xenon (see line b of Figure 4): an initial decrease reaching the minimum at a pressure of 40 kPa, and then an increase is observed. Similar to the behavior of xenon adsorbed in zeolites, a parabolic correlation $\delta = f([Xe])$ is found which is usually ascribed to the presence of strong adsorption sites according to the term $\delta_{S\Lambda S}$ in eq 1.

The interactions of xenon with the MOF surface are also reflected in the line shape. Even by using the MAS technique it is apparent that both lines exhibit a chemical shift anisotropy deriving from the asymmetry of xenon electron cloud interacting strongly with the surface and the Cu^{2+} ions, respectively, because it is well known that paramagnetic centers lead to a NMR line broadening. Besides the influence of the term $\delta_{S\Lambda S}$ the term δ_M plays a more important role in the $Cu_3(BTC)_2$ material contributing to obtained findings, which could not totally be averaged by MAS. In the pressure range between 5 and 40 kPa a line broadening of the peak assigned to the smaller pores is observed during the line width of the other signal is much smaller. Above 40 kPa one can see that a change in the line width takes place which can be attributed to the specific interactions of xenon with the paramagnetic centers. Obviously, if the number of xenon atoms is reduced they have a greater affinity to the Cu^{2+} ions. Generally, the NMR studies demonstrate the appearance of two separate signals over a wide range of xenon pressure suggesting that there is no direct communication between the two different types of pores.

Another adsorption behavior of xenon is found in the $Cu_3(BTC)_2$ sample B as it is seen in the ^{129}Xe NMR spectra shown in Figure 5. Since there are obviously residual solvent molecules inside the pores the ^{129}Xe NMR spectra exhibit only one sharp signal over the whole range of adsorption pressure. The chemical shift increases linearly with higher adsorption pressure of the xenon. The comparison with the obtained chemical shift of the

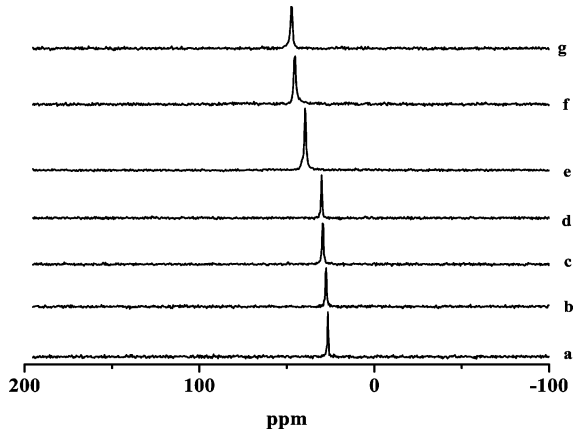

Figure 6. Pressure-dependent ^{129}Xe NMR spectra (performed at room temperature) of xenon coadsorbed with ethylene on $Cu_3(BTC)_2$ sample B: (a) 10 kPa Xe + 10 kPa ethylene, (b) 20 kPa Xe + 20 kPa ethylene, (c) 30 kPa Xe + 30 kPa ethylene, (d) 40 kPa Xe + 40 kPa ethylene, (e) 50 kPa Xe + 50 kPa ethylene, (f) 65 kPa Xe + 65 kPa ethylene, and (g) 75 kPa Xe + 75 kPa ethylene.

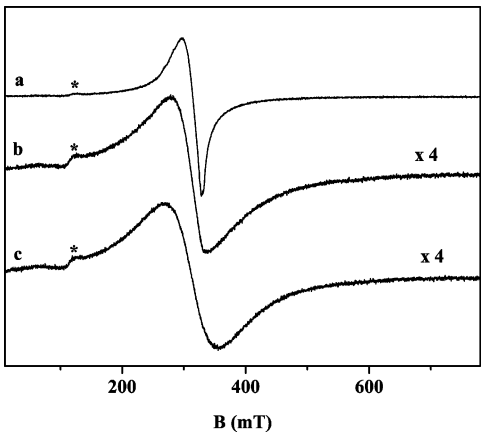

Figure 7. ESR spectra of $Cu_3(BTC)_2$ sample A at (a) 7, (b) 120, and (c) 297 K. The shoulders indicated by asterisks are due to a signal from the cryostat quartz dewar.

$Cu_3(BTC)_2$ sample A demonstrate that the smaller pores must be totally filled by residual solvent molecules and therefore the xenon can only penetrate in the larger pores. Furthermore, the relatively narrow NMR signals and the improved signal-to-noise ratio give rise to the assumption that the interactions between the surface, the Cu^{2+} ions, and the xenon atoms are also reduced, which is a hint that there are residual solvent molecules occupying the strong adsorption sites including the Cu^{2+} ions of the material. This in a good agreement with the results of the thermal gravimetric measurements.

From rehydration experiments,[21] it is known that the $Cu_3(BTC)_2$ material has the capacity to adsorb more solvent molecules as one can remove by thermal treatment. Therefore, we made coadsorption experiments with ethylene as a small molecule and xenon applying equal loading pressures for both gases to study the influence on the NMR results. Under the fast exchange conditions given at room temperature, the observed chemical shift is the weighted average value of the xenon in the pores which can be expressed as follows

$$\delta_{obs} = \frac{N_1}{N}\delta_1 + \frac{N_2}{N}\delta_2 \qquad (2)$$

where δ_{obs} is the observed chemical shift in the porous system, δ_1 and δ_2 ($\delta_1 > \delta_2$) are the chemical shifts in the different pores, N is the total number of adsorbed xenon, and N_1 and N_2 are the populations of xenon adsorbed in the smaller and larger pores of the MOF, respectively. It is seen from eq 2 that, if the proportion of adsorbed xenon is varied, the obtained chemical shifts must be changed. A decrease in the number of xenon atoms in the pores should cause a high-field shift of δ_{obs} when δ_1 is much larger than δ_2. Generally, the adsorption of different sizes of guest molecules in microporous materials is a conventional technique to estimate the pore size. Small molecules such as ethylene will be preferentially trapped in the micropores, and only a limited number of xenon atoms should be adsorbed in these pores yielding to a decrease in the ^{129}Xe NMR chemical shift.

Figure 6 shows the ^{129}Xe NMR spectra of coadsorbed ethylene and xenon into the $Cu_3(BTC)_2$ sample B. Over the entire pressure range only one sharp signal is detected shifted to high-field range which can be assigned to the larger pores of the $Cu_3(BTC)_2$. Again, with increasing loading pressure an increase of the chemical shift is observed but only one signal is seen even at higher xenon pressures. This result suggests that the smaller pores are filled with the residual solvent molecules from the synthesis and additionally adsorbed ethylene (with a kinetic diameter of 3.9 Å[25]). Therefore, these pores are not accessible for the xenon atoms. The comparison of the ^{129}Xe NMR chemical shifts of the coadsorption and the xenon adsorption experiment shows that both are quite similar in the pressure range between 10 and 40 kPa (see Figure 4). Although the absolute xenon pressure in the coadsorption experiments is only the half of the total loading pressure the presence of the ethylene molecules and residual molecules such as water (with a kinetic diameter of 2.65 Å[26]) cause this findings because these substances are trapped in the pores too. Thus, this fact leads to a decrease of mean free path l of xenon and as a consequence to an increase of the corresponding ^{129}Xe chemical shifts despite a lower number of adsorbed xenon atoms. A small downfield shift can be estimated up to 6 ppm if the loading of xenon atoms (pressure of 50 kPa and higher) is further increased. On the results of the coadsorption experiments, it can be estimated that the size of the smaller pores is close to 7 Å because of the mentioned kinetic diameters of ethylene and water, respectively. Thus, it is impossible for the xenon atoms (kinetic diameter of 4.4 Å) to diffuse in these pores. Furthermore, it can be concluded that the pore size of the larger pores is close to 11 Å, which is in good agreement with the results of the nitrogen adsorption experiments (estimated pore diameter of 10.7 Å). The larger pores are formed by primary building blocks and connected through the trimesic acid into a three-dimensional network as shown elsewhere.[21] According to the crystal data one can assume that the smaller pores are formed by secondary building units with other units through corner sharing of the Cu^{2+} dimers.[27] This fact confirms the result that those pores are filled with residual molecules because of the stronger interactions with copper ions.

The ^{129}Xe NMR signals of sample A (see Figure 3) show substantial line broadening effects and downfield shifts in comparison with the sample B, which are presumably caused by the interaction of the adsorbed Xe atoms with paramagnetic copper ions of the $Cu_3(BTC)_2$ framework. Therefore, EPR experiments are performed between 7 and 297 K in order to characterize the state of the copper ions in this material. Figure 7 illustrates three representative EPR spectra recorded at 7, 120, and 297 K of evacuated $Cu_3(BTC)_2$ sample A. At low temperatures, the anisotropic EPR powder pattern of monomeric Cu^{2+} (electron spin $S = {}^1/_2$) species is observed (Figure 7a) where the spectrum appears to be seriously broadened by g and A strain

effects and in particular dipolar spin−spin interactions between the Cu^{2+} ions due to high local concentrations. Therefore, we can only give a rough estimate of the Cu^{2+} spin Hamiltonian parameters $A_{||} = 160 \times 10^{-4}$ cm^{-1}, $g_{||} = 2.35$, and $g_{\perp} = 2.06$. We assign these Cu^{2+} ions to residual extraframework cupric ion species in either an elongated distorted octahedral or square pyramidal coordination,[28,29] which have not been transformed to binuclear Cu^{2+} carboxylates during the synthesis. At intermediate temperatures of about 120 K, a new broad isotropic signal with $g = 2.143$ and a peak-to-peak line width of about 88 mT appears whose intensity is increasing with rising temperature. Such a temperature dependence of the EPR signal intensity is indicative for antiferromagnetically coupled spin system in contrast to the typical Curry-type behavior of the paramagnetic Cu^{2+} monomers. Therefore, we assign this signal to the antiferromagnetically coupled Cu^{2+} dimers with $S = 1$ of the binuclear Cu^{2+} carboxylates building units of the $Cu_3(BTC)_2$ framework. Indeed a strong antiferromagnetic contribution to the susceptibility of $Cu_3(BTC)_2$ at $T > 80$ K has been reported by Zhang et al.[30] Consequently it seems natural to explain the broadening of the room temperature ^{129}Xe NMR spectra in Figure 3 by a magnetic interaction between the ^{129}Xe nuclei and the Cu^{2+} dimers of the $Cu_3(BTC)_2$ framework. Furthermore we have to note that the EPR spectra in parts b and c of Figure 7 do not show the typical features of an $S = 1$ spin system as observed for a number of different dimeric Cu^{2+} species[31] but only a broad line is detected with a g value corresponding to the average g values of these Cu^{2+} dimers. Therefore, we assume that spin exchange between the interconnected copper dimers is taking place across the BTC linker molecules in the $Cu_3(BTC)_2$ framework leading to an averaging of the anisotropic spectral features of the individual $S = 1$ Cu^{2+} dimer spectra.

Conclusions

First, a MOF is investigated by ^{129}Xe NMR experiments to obtain more information about the porosity of such compounds. Compared with other characterization methods such as XRD and IR spectroscopy as it is described elsewhere,[21] the ^{129}Xe NMR spectroscopy reveals a more detailed description of the porosity of the $Cu_3(BTC)_2$ material. The results demonstrate that in this MOF two pores exist with different pore sizes which can be detected if the material is synthesized as sample A. The coadsorption experiments of sample B show that molecules such as ethylene and water totally block the smaller pores of the $Cu_3(BTC)_2$ and therefore the xenon atoms cannot penetrate in these cavities. Only when the pretreatment procedure leads to a removal of the solvent molecules both pores can be filled with xenon atoms. Furthermore, the coadsorption experiments demonstrate that the ethylene molecules obviously undergo strong interactions with the Cu^{2+} sites, which is indicated by the narrow line widths of the obtained xenon NMR signal. In case that only a small amount of residual molecules remain in the pores of $Cu_3(BTC)_2$ the adsorbed xenon atoms interact stronger with the different adsorption sites which is reflected in a line broadening. In addition to these results the EPR measurements demonstrate that the Cu^{2+} ions as well as monomer or dimer strongly influence the chemical shift and the line width of the adsorbed xenon. Especially if most of the residual molecules are removed the interactions with xenon occur across the linker molecules of $Cu_3(BTC)_2$ framework.

Acknowledgment. The authors thank L. Moschkowitz for assistance in the loading of xenon samples.

Supporting Information Available: Mass fragments of samples A and B. This material is available free of charge via the Internet at http://pubs.acs.org.

References and Notes

(1) Yaghi, O. M.; Davids, C. E.; Li, G. M., Li, H. L. *J. Am. Chem. Soc.* **1997**, *119*, 2861.
(2) Li, H. L.; Eddaoudi, M.; O'Keeffe, M.; Yaghi, O. M. *Nature* **1999**, *402*, 276.
(3) Eddaoudi, M.; Kim, J.; Rosi, N.; Vodak, D.; Wachter, J.; O'Keeffe, M.; Yaghi, O. M. *Science* **2002**, *295*, 469.
(4) Yaghi, O. M.; Eddaoudi, M.; Li, M.; Kim, J.; Rosi, N. *WO 2002/088148* **2002**, University of Michigan.
(5) Chac, H. K.; Siberio-Perez, D. Y.; Kim, J.; Go, Y. B.; Eddaoudi, M.; Matzger, A. J.; O'Keeffe, M.; Yaghi, O. M. *Nature* **2004**, *427*, 523.
(6) Stallmach, F.; Gröger, S.; Künzel, V.; Kärger, J.; Yaghi, O. M.; Hesse, M.; Müller, U. *Angew. Chem.* **2006**, *118*, 2177.
(7) Müller, U.; Schubert, M.; Teich, F.; Pütter, H.; Schierle-Arndt, K.; Pastré *J. Mater. Chem.* **2006**, *16*, 626.
(8) Kitagawi, S.; Kitaura, R.; Nore, S. *Angew. Chem., Int. Ed.* **2004**, *43*, 2334.
(9) Prestipino, C.; Regli, L.; Vitillo, G.; Bonino, F.; Damin, A.; Lamberti, C.; Zecchina, A.; Solari, P. L.; Kongshang, K. O.; Bordiga, S. *Chem. Mater.* **2006**, *18*, 1337.
(10) Chen, B.; Ockwig, N. W.; Millward, A. R.; Contreras, D. S.; Yaghi, O. M. *Angew. Chem.* **2005**, *117*, 4823.
(11) Millward, A. R.; Yaghi, O. M. *J. Am. Chem. Soc.* **2005**, *127*, 17998.
(12) Gonzalez, J.; Devi, R. N.; Tunstall, D. P.; Cox, P. A.; Wright, P. A. *Microporous Mesoporous Mater.* **2005**, *84*, 97.
(13) Loiseau, T.; Muguerra, H.; Ferey, G.; Haonas, M.; Taulelle, F.; Ito, T. *J. Solid State Chem.* **2005**, *178*, 621.
(14) Ito, T.; Springuel-Huet, M. A.; Fraissard, J. *Zeolites* **1989**, *9*, 68.
(15) Fraissard, J.; Ito, T. *Zeolites* **1988**, *8*, 350.
(16) Springuel-Huet, M. A.; Sun, K.; Fraissard, J. *Microporous Mesoporous Mater.* **1999**, *33*, 89.
(17) Clewett, C. F. M.; Pietraβ, T. *J. Phys. Chem. B* **2005**, *109*, 17907.
(18) Garsuch, A.; Böhlmann, W.; Sattler, R. R.; Fraissard, J.; Klepel, O. *Carbon* **2006**, *44*, 1173.
(19) Kennedy, G. J. *Polym. Bull.* **1990**, *23*, 605.
(20) Miller, J. B.; Walton, J. H.; Roland, C. M. *Polym. Sci. B* **1992**, *30*, 327.
(21) Schlichte, K.; Kratzke, T.; Kaskel, S. *Microporous Mesoporous Mater.* **2004**, *73*, 81.
(22) Springuel-Huet, M. A.; Bonardet, J. L.; Gédéon, A.; Fraissard, J. *Langmuir* **1997**, *13*, 1229.
(23) Ito, T.; de Menorval, L. C.; Guerrier, E.; Fraissard, J. *Chem. Phys. Lett.* **1997**, *11*, 271.
(24) Ripmeester, J. A. *J. Magn. Res.* **1984**, *56*, 247.
(25) Breck, D. W. *Zeolite Molecular Sieves, Structure, Chemistry, and Use*; John Wiley & Sons: New York, 1974.
(26) Hirschfelder, J. O.; Curtis, C. F.; Bird, R. R. *Molecular Theory of Gases and Liquids*; John Wiley & Sons: New York, 1954.
(27) Chui, S. S. Y.; Lo, S. M. F.; Charmant, J. P. H.; Orpen, A. G.; Williams, I. D. *Science* **1999**, *283*, 1148.
(28) Hathaway, B. L.; Billing, D. E. *Coord. Chem. Rev.* **1970**, *5*, 143.
(29) Tominaga, H.; Ono, Y.; Keii, T. *J. Catal.* **1975**, *40*, 1075.
(30) Zhang, X. X.; Chui, S. S. Y.; Williams, I. D. *J. Appl. Phys.* **2000**, *87*, 6007.
(31) Bencini, A.; Gatteschi, D. *EPR of Exchanged Coupled Systems*; Springer: Berlin, 1900.